Nieto-Villena, A.; Martinez, JR.; Flores-Camacho, JM.; Lastras-Martinez, A.; De La Cruz-Mendoza, JA.; Ortega-Zarzosa, G.; Valcarcel Andrés, JC.... (2018). Infrared Ellipsometry Analysis of Heritage Photographic Prints. Studies in Conservation. 63(8):466-476. https://doi.org/10.1080/00393630.2018.1476962

Infrared ellipsometry analysis of heritage photographic prints

Number of words: 7828

Abstract

Focusing on the photographic archive of Julián Carrillo (México), we study and characterize the photographic process of a set of 13 photographs dated between 1884 and 1925. By using infrared spectroscopic ellipsometry we classified a selected set of photographs according to the kind of binder used. Thus, we recognized for each photograph, the presence of proteins, and thus the particular photographic process. Furthermore, we have identified the presence of baryta layer, the use of plasticizer, and the eventual coating utilized to protect the photograph, whose composition was based in natural organic components, mainly shellac, beeswax, or camphor.

Keywords: ellipsometry; photography; binders; historic archive; characterization; photographic processes.

1. Introduction

Objectively identifying the stratigraphic structures of photographic prints that are found in the processes developed since the invention of photography pose in the present a full challenge, leaving aside the empirical assumptions practiced by experts made by visualization.

Among the processes more common and, incidentally, more demanding to distinguish from each other include the kind of binder used in prints such as, albumen, collodion and both gelatin processes, namely, POP (Printing out Paper) and DOP (Developing out Paper). Additionally, structural differences between them, and the possibility of containing dyes, varnishes, and other physical characteristics, occasionally difficult their identification.

The fragility and vulnerability of both, the photographs' supports and their thin strata, prevent the analyst from performing a simple identification. The experimental techniques more commonly used in laboratory and conservation workshops are either destructive or insufficient.

For the preservation of early 20th century, late 19th century photographs, it must be considered that photographs consist of multi-layer systems made up of complex mixtures of inorganic and organic materials.

A number of working methods have been developed and introduced to aid in the identification of photograph processes (Coe and Haworth-Booth 1983; Sammlung, Knodt, and Pollmeier 1999; Reilly 1986). Fourier transform infrared (FTIR) spectroscopy in either transmission mode or attenuated total reflection (ATR), and Micro FTIR have been used to detect organic compounds in photographs (D. Stulik et al. 2002; McCabe 2005; Gernsheim 1965; Casoli and Fornaciari 2014; Ricci, Bloxham, and Kazarian 2007; Cattaneo et al. 2008).

The employment of infrared absorbance spectroscopy provides information on the structural and compositional properties of the binder, whose use was necessary at the time to protect silver particles from air pollution or other substances present in adjacent materials, attempting thus, to preserve the images from oxidation and any other kind of deteriorating processes (Gernsheim 1965; Casoli and Fornaciari 2014).

Collodion presents a set of typical absorption bands centered at about 1300, 1680, and 880 cm^{-1}, which are attributable to the presence of a plasticizer commonly used during the preparation of the collodion emulsion. These bands are used as fingerprints of the nature of the binder (Ricci, Bloxham, and Kazarian 2007; Cattaneo et al. 2008).

In techniques where infrared absorption spectra are obtained from diffuse reflectance, the presence of paper interferes with the resultant spectra by combining absorption features originating from both, the binder and the paper, as a background signal, that can produce broadening of the bands and a general loss of resolution, particularly at the lower frequency end.

In our case, we analyze photographic positive prints, thus, to prevent loss of information about the natural organic layer used as a binder coating, we employed infrared spectroscopic ellipsometry technique, which can help us to resolve the infrared absorption bands and, based

in the absence or presence of principal vibrational bands as main criteria, distinguish the organic compound used. As far as we know, infrared spectroscopic ellipsometry has not been used as a characterization technique for photographic processes.

Infrared Spectroscopic Ellipsometry (IRSE) in the spectral range from 300 to 4000 cm^{-1} (33 to 2.5 μm. Such wavelengths are within the mid-infrared range of the electromagnetic spectrum) was used as the characterization tool in the present work. This optical technique can be broadly described as follows (Fujiwara 2007): a well-defined linear polarized light impinges a sample at oblique incidence, upon reflection the polarization state changes, in general, from linear to elliptic. The change in polarization state carries with it information on the dielectric properties of the sample. The determination of the reflected polarization state is made by means of optical modulation techniques, resulting, for each wavelength, in a set of two data measured simultaneously without need of cumbersome mathematical post processing. This pair of data are the relative change in amplitude and the relative change of phase of the light upon reflection with respect to the incident polarization state. In the literature they are called, respectively, Ψ and Δ. For the present study, we have chosen to convert these data pairs to a representation known as effective-dielectric function $\langle\varepsilon\rangle$, which is a complex number consisting on a real part, $\langle\varepsilon_1\rangle$, and an imaginary part $\langle\varepsilon_2\rangle$, where the latter could in principle, under some circumstances, as we discuss next and later in the results section, be directly related to absorption.

Ellipsometry can be used to distinguish individual layers in a stratified system such as the photographic prints presented here. This could be done by means of ideal models, which when feasible, permit obtaining the complex dielectric function of the layer constituent and its thickness. However, as photographs are far from being ideal systems, a model cannot be accurately applied, but, the overall line shape permits performing a quantitative analysis of constituents' vibrational modes and a qualitative estimation of the stratified structure of photographic prints: the expected complex line shape of $\langle\varepsilon\rangle$ near resonance frequencies is a Lorentzian curve composed of a peak centered at the characteristic absorption of the material (imaginary part), and a line resembling a simple oscillation crossing zero (or its baseline) when its partner passes its maximum (real part). For simple, isotropic media $\langle\varepsilon\rangle$ corresponds

one-to-one to the actual dielectric function ε. For stratified samples this relationship is no longer expected to be one-to-one, the real and imaginary parts can be interchanged in such a way that the absorption peak is revealed in the $\langle \varepsilon_1 \rangle$ component of the signal. This interchange depends on the strength of the resonant feature, the wavelength, and how deep its originating layer is buried in the stratified system.

A further advantage of this technique, is that, since it measures relative changes in the polarization state, the acquired data carry information only from the sample without being affected by the surrounding environment, such as ambient air, which in principle can distort absolute infrared measurements.

The purpose of the present work is to recognize the composition of ancient photographs from the reserve of the Centro Julián Carrillo's photographic archives (Mexico), which register the musician's academic and artistic live around the world during the late 19th and 20th centuries. Carrillo introduced the 13^{th} sound theory, based on the actual microtonal music. From a chemical point of view, an integrated analytical approach based on the use of non-destructive and non-invasive techniques is required to identify different photographic techniques. The identification of materials, in particular, is a fundamental step to individuate the right way to preserve photographs and, if necessary, to plan an adequate restoration method. In this sense, the precise knowledge of substances, causes and implicated processes guarantees an appropriate and conscious approach decisive for the good recovery, protection and conservation (Casoli and Fornaciari 2014; Cattaneo et al. 2008; Hendriks and Ross 1988; Ostroff 1966; Hogan, Golovlev, and Gresalfi 1999; Golovlev et al. 2003).

2. Experimental

A representative group of 13 historic photographs belonging to the Julián Carrillo historical archive has been selected for analysis. The fact that these photographs were processed in different countries, during the years of exploration of a broad range of techniques by artists and professionals, has allowed us to have a significant set of samples for our purposes.

In figure 1 we show the aforementioned set of photographs. From the archive's records, the subject's dress and discernable details of the photographer's studio on the image, the photographs are dated and situated as follows: JC-03, La Habana (1925). JC-04, Mexico (1884). JC-05, Mexico (1909); JC-12, unknown origin (1895). JC-13, Leipzig (1900). JC-14, Paris (1900). JC-15, Paris (1900). JC-16, Brussels, (1903). JC-17, Paris (1899). JC-18, Brussels (1905). JC-19, México (1907). JC-20, México (1907). JC-29, Ahualulco, Mexico (1890). We are numbering the samples in accordance to the Julian Carrillo Center filing protocols.

Figure 1. Set of 13 photographs from the Centro Julián Carrillo archives (Mexico) selected for this study.

IRSE measurements were carried out with a commercial apparatus (IR-VASE from J.A. Woollam Co. USA) equipped with dedicated infrared optics, including an automated rotating compensator for the modulation mentioned above. The monochromatic light is provided by an incandescent solid element and an integrated Michelson interferometer.

Raman spectra were acquired with the aid of a confocal microscope using a commercial instrument (alpha 300, from WITec, Germany). For the excitation source, a 633 nm He-Ne Laser was employed. For the detection of the thin baryta layer, we used a 100 X objective and a laser power of 36 μW. This low laser power prevents damage of the samples studied in the present work and quenches effects of fluorescence and luminescence that overcome the response of spectral features of interest. Furthermore, the high spatial resolution allowed by the confocal microscope permits scanning the sample in different directions, even vertically into the samples, a characteristic used for this paper.

3. Results

The early photography process used a great variety of materials in complex combinations to obtain an image print. Among the used materials, we can observe binders, which form part of the emulsion, elements present in other layers such as paper carrier cellulose or barium sulfate present in the baryta layer and other coating materials, plasticizers or aggregates. In the emulsion binder we can encounter either albumin, collodion or gelatin. Other strata as barium sulfate or cellulose can be present as well. Furthermore, in some samples we can find protective coating surface compounds such as shellac, gum arabic, beeswax or linseed oil, and the presence of plasticizers and other aggregates, as camphor, castor oil, glycerin, starch or casein. Thus, the identification of the complete structure of ancient photographs is complex. Commonly, the characterization work of the chemical compounds in photography samples is focused on the identification and differentiation of the binder, thus the main identification criterion consists on comparing the intensity of the absorption bands of amides in the spectral region between 1250 cm^{-1} and 1750 cm^{-1} (Casoli and Fornaciari 2014; Ricci, Bloxham, and Kazarian 2007).

The characterization of proteinaceous binder has been traditionally possible by comparing intensity of the bands at about 1450 cm^{-1} and 1410 cm^{-1}, as follows: If the intensity of the band at 1410 cm^{-1} is larger than that of the band at 1450 cm^{-1}, the binder is identified as albumen, whereas, if the opposite is true, the binder is recognized as gelatin (Casoli and Fornaciari 2014). However, in some cases this peak ratio comparison criterion is not conclusive, and the ambiguity makes it difficult to differentiate the binder present in the photographic process.

Collodion presents a typical peak at 1300 cm^{-1} on its own. An absorption peak at 1723 cm^{-1} also present in collodion photographic material can be, however, assigned to the presence of a plasticizer which was added to the collodion emulsion during its preparation (Ricci, Bloxham, and Kazarian 2007; Cattaneo et al. 2008).

In general, the spectra depend on the sample aspect, age and degradation. The analyzed photographs show natural ageing effects and some physical degradation that implies deeper structural degradation. Thus, discerning between compounds could be ambiguous. Also, in techniques where spectra are obtained from diffuse reflectance, the presence of the paper substrate interferes with the results, by convoluting its response with that from the binder. This is noticed by the broadening of the bands, and consequently a general loss of resolution in the relevant frequency range where the features originating from natural organic components as resins, gum, oils, and waxes, used mainly as coating layer, could be observed (Perron 1989). Thus, it is recommended the combined use of Raman and IR spectroscopies to discriminate between organic compounds used in the photograph process. In our case the use of infrared ellipsometry can help us to resolve the infrared absorption bands and, based in the absence or presence of principal bands as main criteria, discriminate through photographic techniques.

In the spectrum of sample JC-03 shown in figure 2, we can clearly identify in the range between 1800 and 1400 cm^{-1} the signals corresponding to the amide groups characteristic of the protein materials. The peak at 1638 cm^{-1} is attributed to stretching vibrations of C = O bonds. The peak at 1547 cm^{-1} to N-H bending vibrations with stretching C-N, are the so-

called amide I and II, respectively. The following two signals at 1453 and 1406 cm^{-1}, corresponding to the bending mode of the C-H group, belong to the amide III. The relative intensities of these two features allows us to differentiate the kind of binder. Thus, for JC-03 we identified the presence of gelatin. This observation is confirmed by the presence of the signals from C-H stretching vibrations located at 3072, 2947, and 2874 cm^{-1}, observed in figure 2(c), which also correspond to gelatin (M. R. Derrick, Stulik, and Landry 2015).

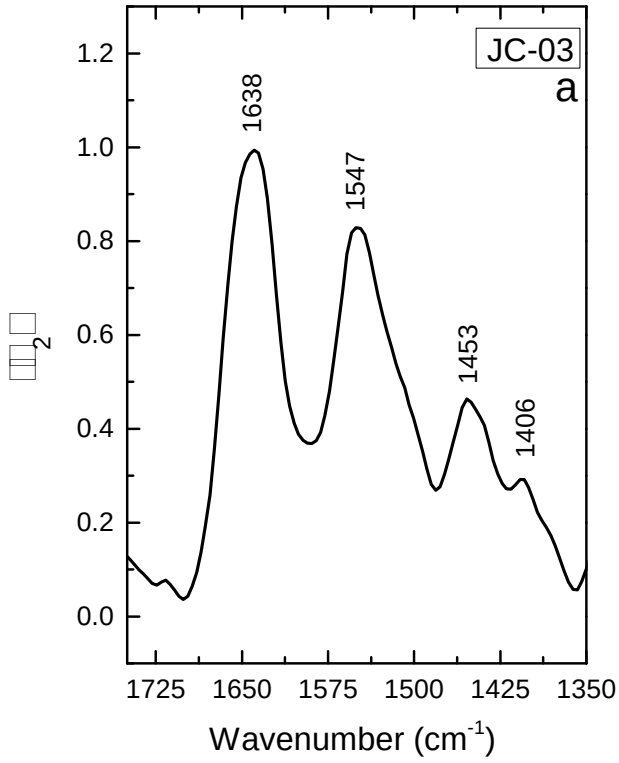

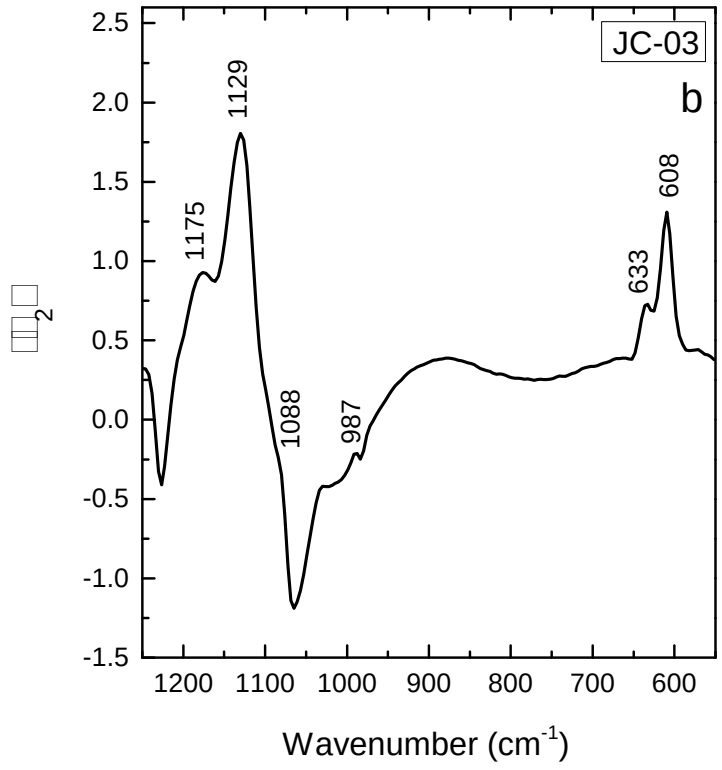
JC-03
b
1129
1175
1088
987
633
608
2.5
2.0
1.5
1.0
0.5
0.0
-0.5
-1.0
-1.5
1200
1100
1000
900
800
700
600
Wavenumber (cm-1)

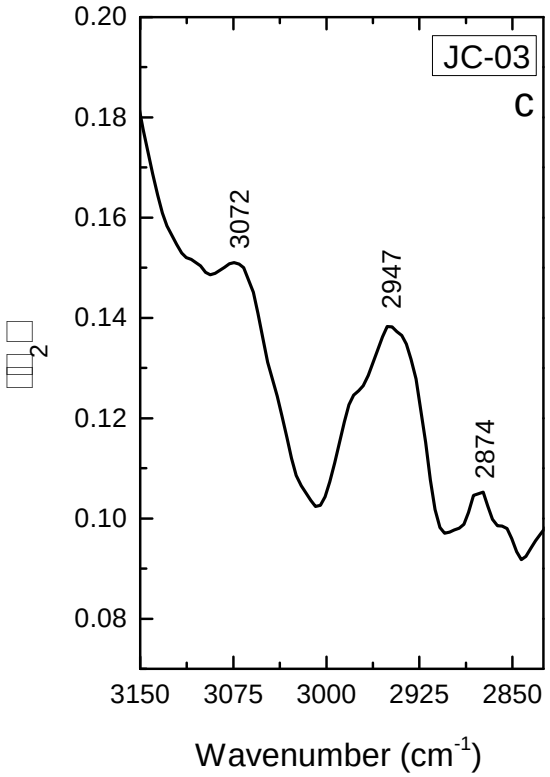
JC-03
c
3072
2947
2874
0.20
0.18
0.16
0.14
0.12
0.10
0.08
3150
3075
3000
2925
2850
Wavenumber (cm-1)

Figure 2. IRSE spectra of the photograph JC-03 in the regions 1350 cm^{-1} to 1750 cm^{-1} a), 550 cm^{-1} to 1250 cm^{-1} b), and 2825 cm^{-1} to 3150 cm^{-1} c).

Samples JC-03, JC-04, JC-05, JC-12, JC-20 and JC-29 show the same behavior in the spectral regions shown for JC-03 in figure 2, therefore their binder can be classified as gelatin.

These analyzes have made it possible to discern with greater certainty, which to the best of our knowledge have not been reported so far in the scientific literature, between the different binders. This relationship is formed through the presence of other strata present in the processes that contain gelatin but not albumin. We refer to the baryta layer that was applied between the cellulosic support and the binder.

This layer is composed of $BaSO_4$ and a small proportion of gelatin and has been identified through the manifestation of vibrational modes attributed to presence of barium sulfate.

In the case of the sample JC-03 we find signals at 1175, 1129, 1088, and 987 cm^{-1} corresponding to the symmetrical stretching vibration of S-O assigned to the presence of SO_4 and at 633 and 608 cm^{-1} to the bending vibration of SO_4. We can find others at 2087 and 2061 cm^{-1}, which correspond to stretching and bending vibrations of sulfur-oxygen bonds (Ramaswamy, Vimalathithan, and Ponnusamy 2010; Sifontes et al. 2015).

In figure 2b, the stretching vibrations of S-O located at 1175, 1129 and 1088 cm^{-1} have been assigned to barium sulphate even though some of them may coincide with cellulose. However, the stretching vibrations bands of S-O at 633, and 608 cm^{-1} are very distinctive of barium sulphate. These characteristics are also present in samples JC-05, JC-12, JC-20, and JC-29. Therefore, these samples contain the baryta layer as well.

The binder of photograph JC-04 has been classified as gelatin, as can be observed in figure 3A, where the peak at 1450 cm^{-1} is higher than the peak at 1410 cm^{-1}. Additionally, we can

identify the presence of peaks related to the presence of bone black pigment located at 1154, 1056, 1030, and 603 cm^{-1}, ("The Infrared and Raman Users Group (IRUG)" 2009). These features are indicated in figure 3 with (b) labels. Thus, this photograph was performed with a carbon process. For comparison of IRSE with traditional techniques, we conducted parallel infrared absorption measurements in reflection mode employing a micro FT-IR Bruker Vertex 70 spectrometer, with a RockSolid^{TM} interferometer using a Hyperion Bruker microscope directly on photograph samples. The infrared absorption spectra obtained from diffuse reflectance yield, besides of the broadening of the bands, a general loss of resolution at the lower frequency end, as can be shown in figure 3B where we show an infrared absorption spectrum, in which the peak at 603 cm^{-1} is absent, while it is detected in infrared ellipsometric spectra, as shown in figure 3A. In samples with natural organic covering the main fingerprint in region from 1000 to 1200 cm^{-1} can be obscured, making thus difficult the identification of the bone black pigment presence; therefore, the infrared spectroscopic ellipsometry technique helps us to resolve the infrared-active bands and to distinguish the used organic compound. As an example, it can be observed in the FTIR measurement shown in figure 3B, that the intensity ratio of amides, labeled with (a) in the figure, does not permit to clearly discern between gelatin and albumen. This ambiguity is, however, resolved with infrared ellipsometry as can be seen in figure 3A, where the intensity of peak at 1450 cm^{-1} is greater than intensity peak at 1410 cm^{-1}, giving us a clear identification criterion as gelatin binder, in this case. A similar situation will be shown below for sample JC-17 which can be identified as albumen.

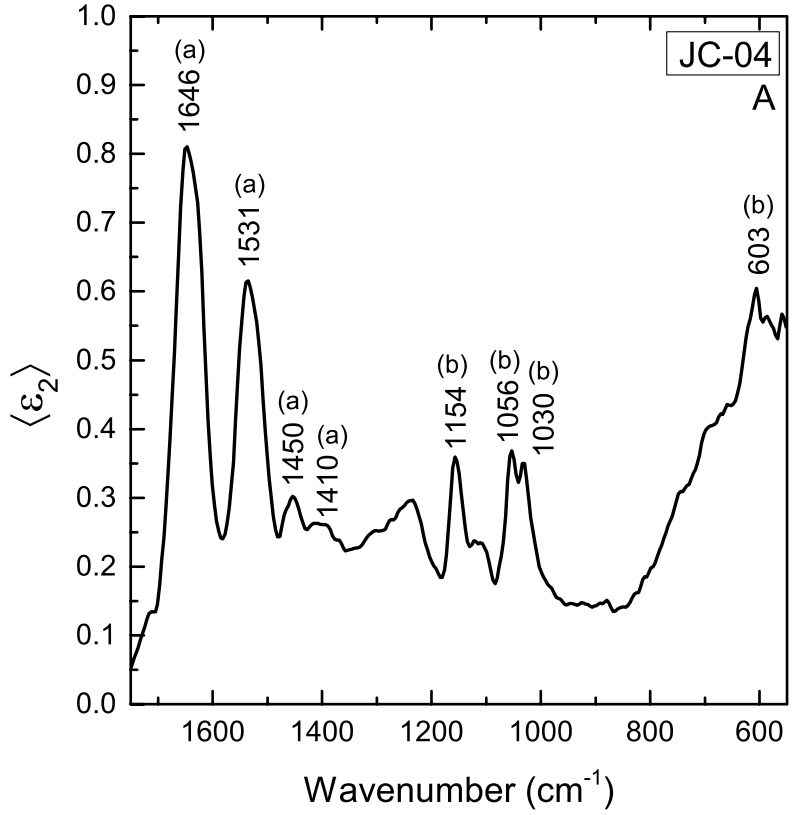
JC-04
A
(a)
1646
(a)
1531
(a)
1450
(a)
1410
(b)
1154
(b)
1056
(b)
1030
(b)
603
⟨ε2⟩
Wavenumber (cm-1)
1.0
0.9
0.8
0.7
0.6
0.5
0.4
0.3
0.2
0.1
0.0
1600
1400
1200
1000
800
600

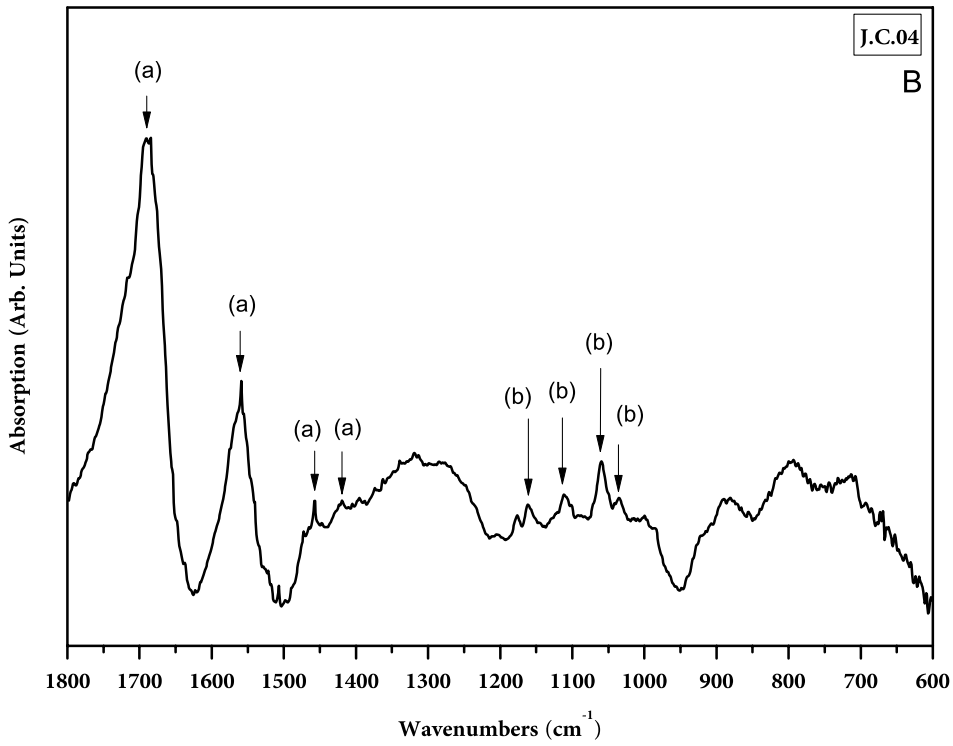

Figure 3. A) IRSE and B) FTIR spectrum of photograph JC-04. Peaks corresponding to bone black pigment are indicated with (b) labels.

In figure 4, we compare the real, $\langle \varepsilon_1 \rangle$, and imaginary, $\langle \varepsilon_2 \rangle$, parts of the infrared ellipsometry spectrum (indeed, an effective dielectric response as discussed in the introduction section) of photographs JC-29 and JC-04 in the region between 600 and 1200 cm^{-1}. The presence of the baryta layer is clearly observed for the spectra of photograph JC-29, and it is notoriously absent in the photograph JC-04. Thus, the JC-04 photograph is carbon print whereas JC-29 photograph is gelatin print (Nieto-Villena et al. 2018).

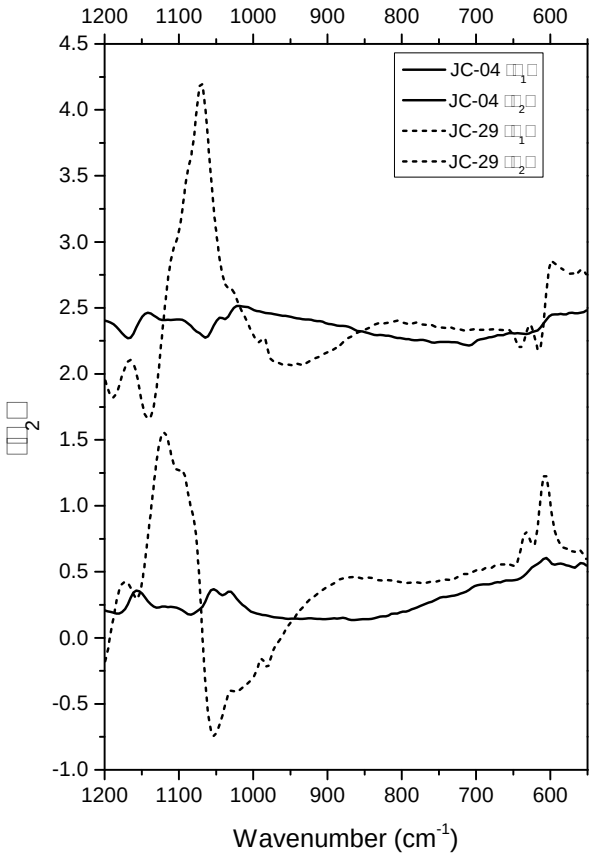

Figure 4. Real, $\langle \varepsilon_1 \rangle$, and imaginary, $\langle \varepsilon_2 \rangle$, parts of the infrared ellipsometry spectrum of photographs JC-29 and JC-04 in the region between 600 cm^{-1} to 1200 cm^{-1}.

It must be noted that the signals corresponding to the baryta layer present the typical behavior of a buried layer. The contribution of absorption around 1088 cm^{-1}, i.e., "the peak", is revealed in the real part of $\langle \varepsilon \rangle$, whereas the absorption peaks at around 633 and 608 cm^{-1} are manifested in $\langle \varepsilon_2 \rangle$. This is an important highlight concerning the degree of sensitivity of the ellipsometry technique proposed in this work: it does not only provide information concerning the constituent materials, but also, thanks to measurements of amplitude and phase, information on the layered structure of photograph prints. We will provide further details in an upcoming publication.

For the JC-12 photograph, which we have already classified as gelatin, we find some differences with respect to the other gelatin prints in the spectral region between 600 and 1300 cm^{-1}. The main differences, as shown in figure 5, are the sharp absorption band appearing at 1217 cm^{-1} corresponding to ester, acid, and alcohol groups, C-O, and the weak shoulder at around 1715 cm^{-1}. These bands are attributable to the presence of a coating layer, possibly shellac.

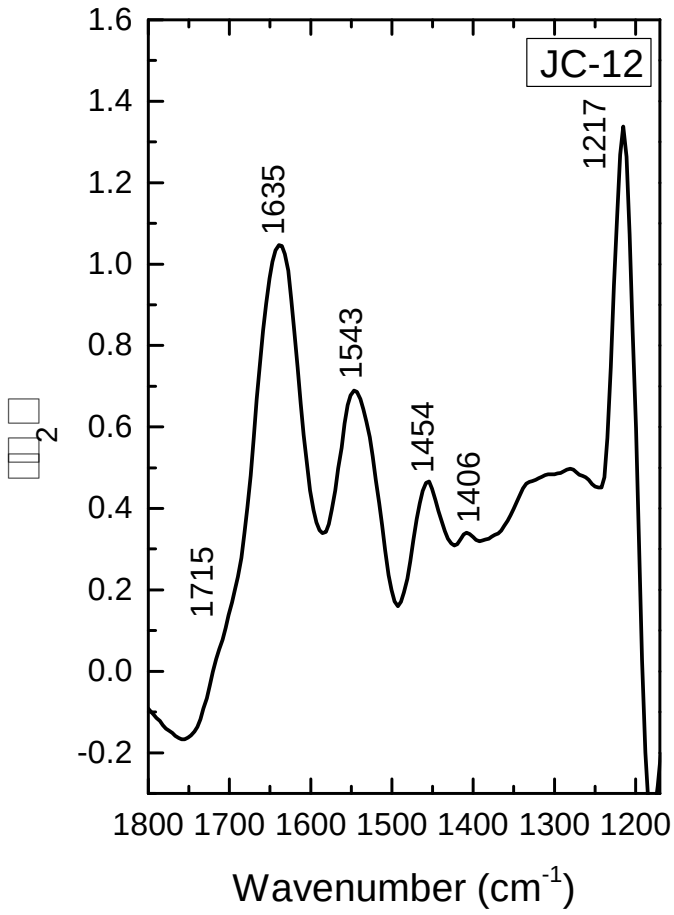

Figure 5. IRSE spectra for the photograph JC-12 in the region 1150 cm^{-1} to 1800 cm^{-1}.

This compound has two strong signals around 1712 and 1730 cm^{-1} from C = O stretching bands. However, with the strongest amide I signal of gelatin at 1635 cm^{-1}, we can only deduce the coating layer through a weak shoulder barely arising to the left of amide I.

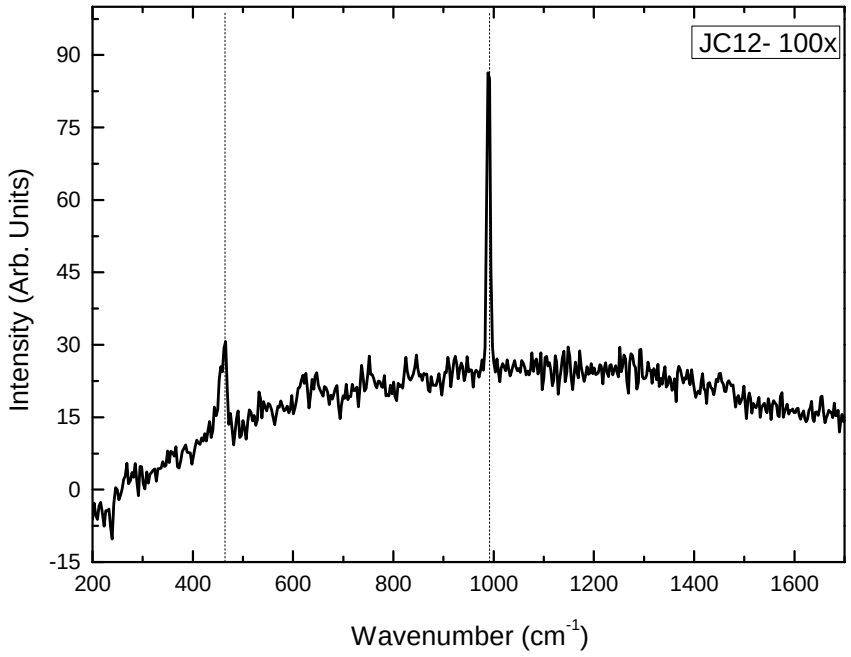

Figure 6. Raman dispersion for the photographs JC-12.

On the other hand, we observe the presence of natural organic components, i.e. the resin shellac in the sample JC-12. Insect resins, as shellac, are mixtures of esters of fatty acids. Acids, such terpenic acid, play an important role in their oxidation (Daher et al. 2010; Mallégol, Gardette, and Lemaire 2000). Shellac was used to enhance and preserve paintings and photographs (Edwards, Farwell, and Daffner 1996; Othmer 1990).

The distinction between gelatin and albumen is a more delicate one. Both, being proteins, show strong amide I and amide II bands in the same frequency range. However, the intensity ratio and shifts of the amide III bands, can be used as identification criteria: albumen band of amide tends to shift to lower frequencies, whereas in gelatin the amide bands were always at

the same frequencies (Perron 1989). We propose an additional criterion consisting on the absence of baryta layer for albumen process.

Figure 7 shows the absorption bands of sample JC-13, where we can observe the amide I groups (about 1630 cm^{-1}), amide II (1542 cm^{-1}) and two amide III related peaks (1450 and 1410 cm^{-1}). The ratio of the amide III peak intensities is smaller than 1, which leads us, therefore, to identify the protein binder as albumen (cf. Fig. 7b).

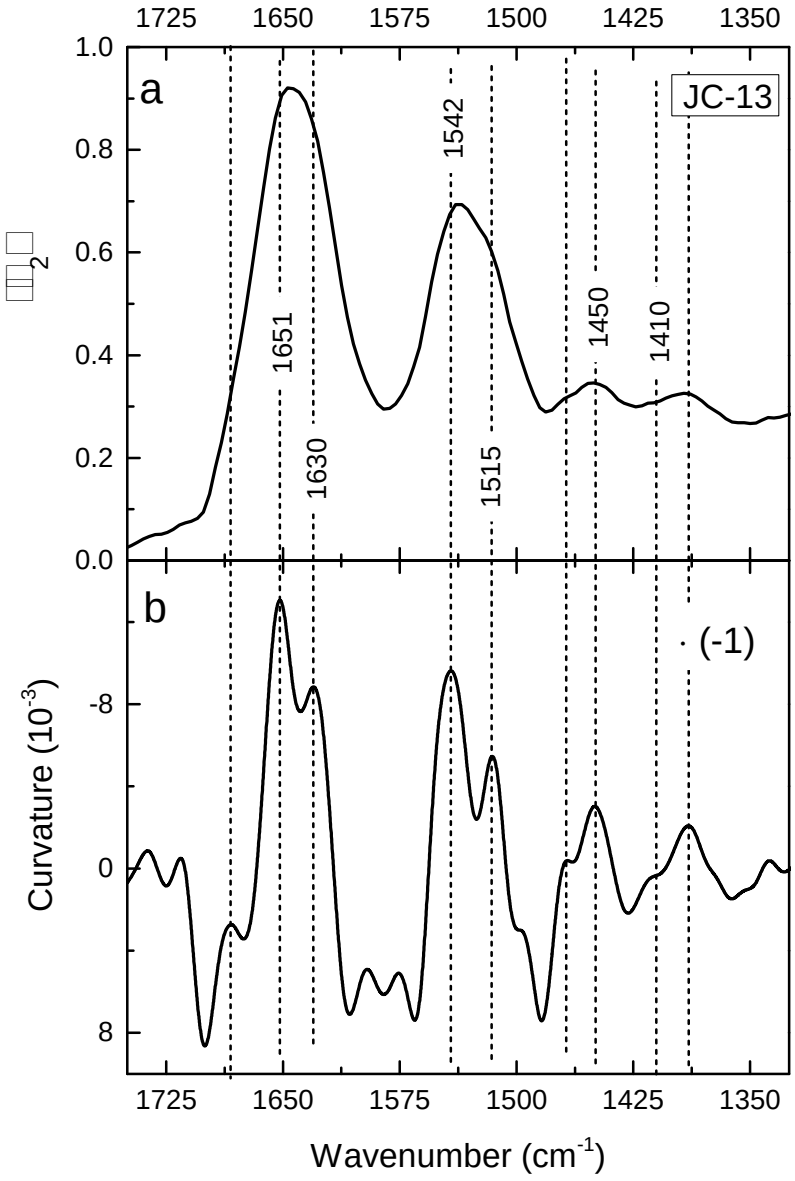

Figure 7. IRSE spectra of the photograph JC-13 in the spectral region from 1350 to 1750 cm^{-1}

In figure 7(b) we show a further proposal of spectral analysis. By taking a second order derivative of a spectrum (with respect to its abscissa, either wavenumber or wavelength) we obtain a local value of the curvature of the spectrum. The important point here is that such an operation brings with it an enhancement of line shapes without altering peak positions. With it, for example, shoulders can be separated from a dominant peak. This helped us to evaluate with more certainty the amide III ratio.

Another element that helps to confirm the identification of JC-13 as albumen print is the absence of signals corresponding to barium sulfate, this is shown in figure 8, where we compare the JC-13 spectrum with one of a sample with the baryta layer such as JC-29.

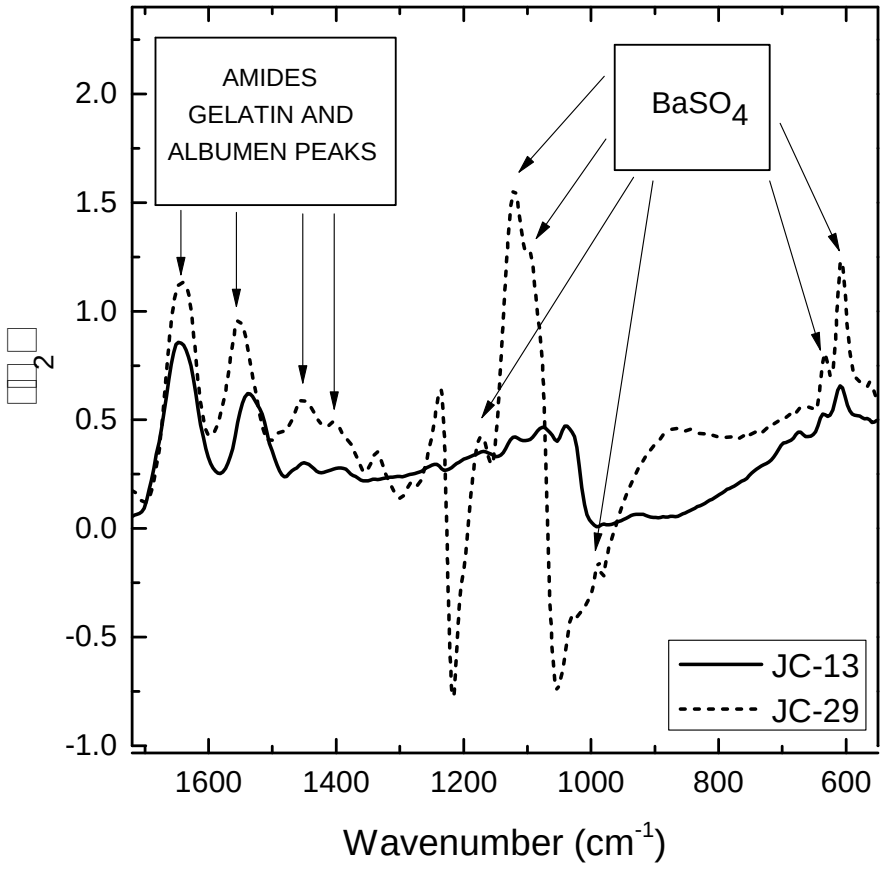

Figure 8. Comparison of IRSE spectra for the photographs JC-13 and JC-29 in the spectral region from 550 to 1700 cm^{-1}.

In the spectral region corresponding to the amide III, we can observe other absorption bands which can be assigned to the presence a beeswax, (see figure 7). Small and sharp doublets between 1466 and 1462 cm^{-1} and between 730 and 720 cm^{-1} are characteristic of the semi-crystalline structure of waxes (M. R. Derrick, Stulik, and Landry 2015). The broad band observed in figure 8 centered at 730 cm^{-1} indicates that there are at least 4 methylene groups in the chain. Beeswax has a high percentage of aliphatic esters and the band of ester groups are represented in the weak stretching band C = O at 1740 cm^{-1} and for the C-O band in the 1175 cm^{-1} region (Brambilla et al. 2011).

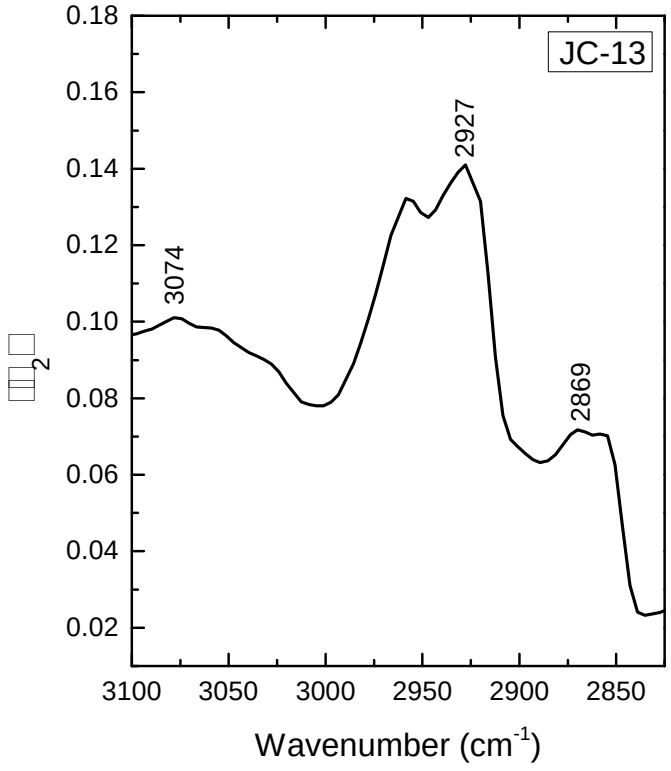

Figure 9. IRSE spectra of the photograph JC-13 in the spectral region from 2825 to 3100 cm^{-1}.

Beeswax, the most commercially important of animal and insect waxes, is obtained mainly from the domesticated honey bees, *Apis mellifica*, which produces the wax as a digestive secretion from flower pollen (Edwards, Farwell, and Daffner 1996). We identified its use in photograph process that is presents in albumen prints.

We can propose, then, the detection of the presence of baryta layer as a criterion to distinguish the kind of binder present in the photographic process. Its absence give us a clear hint for the usage of the albumen print method, whereas its presence is associated to gelatin or collodion print.

In the case of samples JC-16, JC-18, and JC-19 we identify the emulsion binder as collodion. Figure 10 shows absorption spectra of one of these samples, as a typical example, since they are essentially similar, except for minor intensities for the sample JC-19. We can highlight the peaks (c) in 1647 cm^{-1}, 1214 cm^{-1} (N-O stretching bands), 1033 cm^{-1} (C-O bending) and 839 cm^{-1} (N-H bending). We can also associate to the presence of this compound the signals at 2930, 2666 cm^{-1} not shown in the figure.

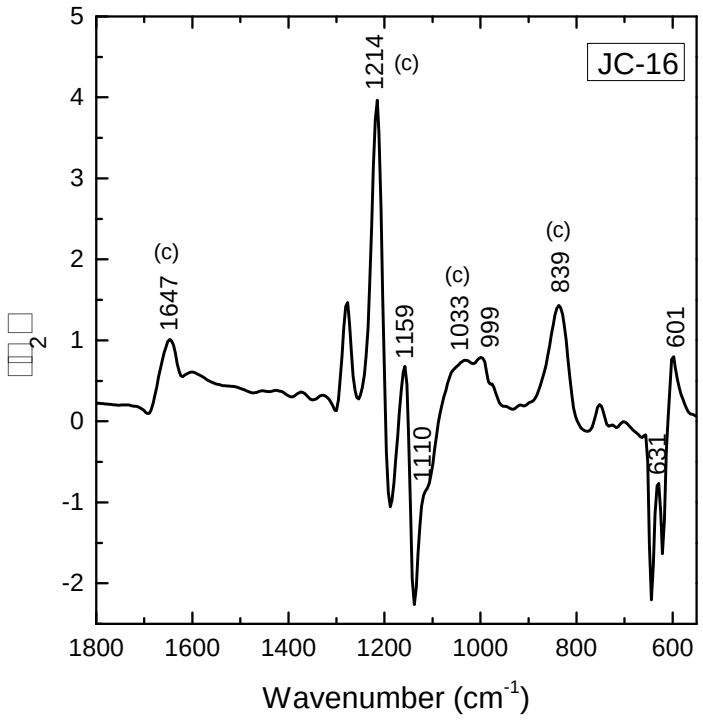

Figure 10. IRSE spectra of photograph JC-16 in the spectral region from 550 to 1800 cm^{-1}.

The peaks at 1718, 1268, 1038, 919, and 945 cm^{-1} are associated to the presence of some plasticizer (probably camphor) which was commonly added to cellulose nitrate to improve its physicochemical properties and to prolong both their useful life, by stabilizing it, and transforming it into less brittle (M. R. Derrick, Stulik, and Landry 2015). The shoulder around 1718 cm^{-1} corresponds to the strong carbonyl band and its intensity depends on the degree of sublimation and therefore degradation of the compound (M. R. Derrick, Stulik, and Landry 2015).

We have found for the collodion processes, as for gelatin before, the baryta layer. This can be seen in the spectrum in figure 10. The signals in the corresponding bands (1159, 1110, 999, 631, and 601 cm^{-1}) complement the identification of compounds in the present sample.

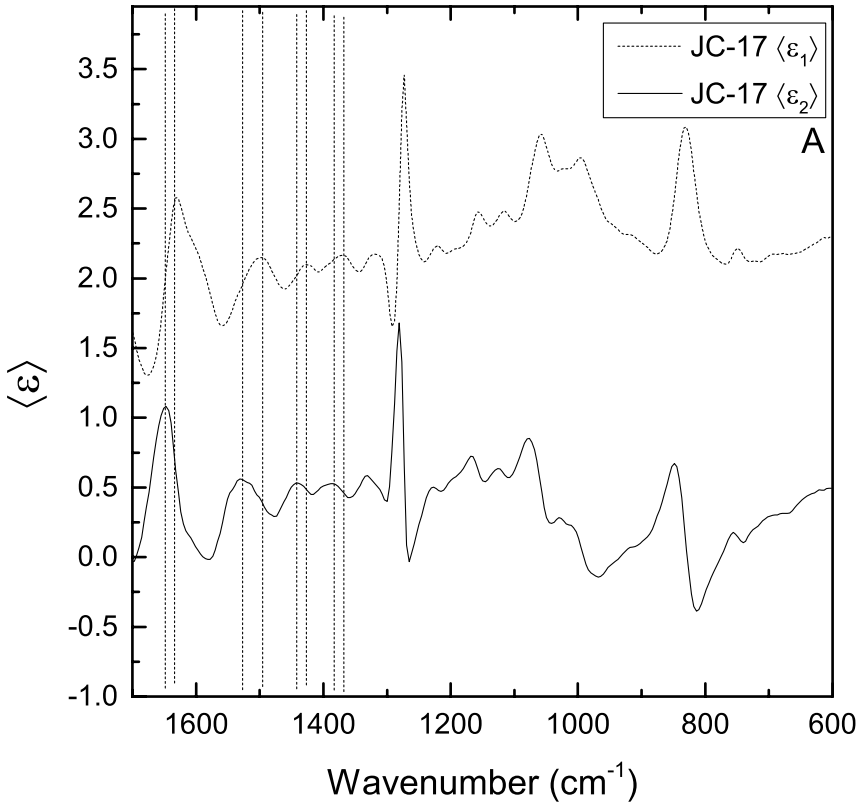
JC-17 ⟨ε1⟩
JC-17 ⟨ε2⟩
A
⟨ε⟩
3.5
3.0
2.5
2.0
1.5
1.0
0.5
0.0
-0.5
-1.0
1600
1400
1200
1000
800
600
Wavenumber (cm-1)

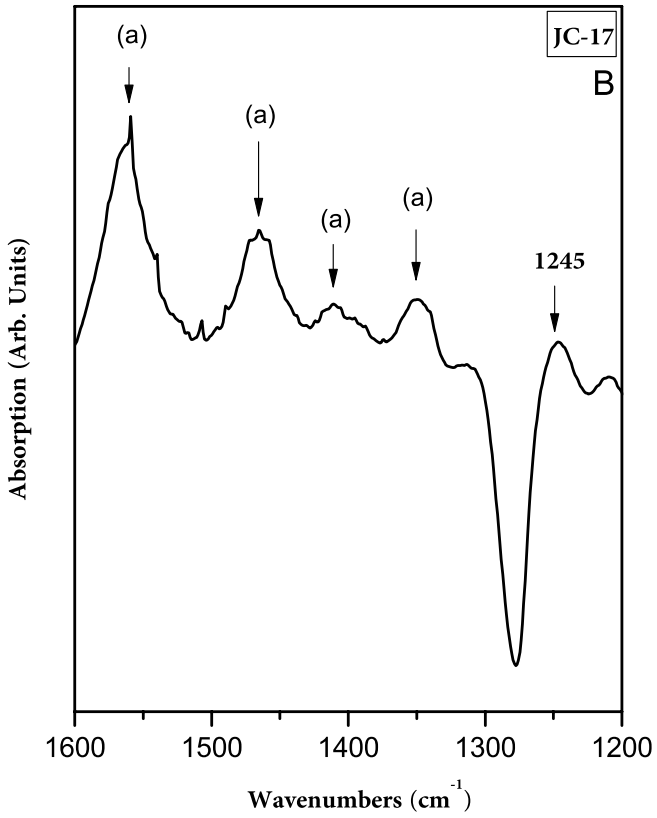

Figure 11. A) Real $\langle \varepsilon_1 \rangle$, and imaginary $\langle \varepsilon_2 \rangle$ parts of the infrared ellipsometry spectrum of photograph JC-17 in the spectral region from 600 to 1700 cm^{-1}, and B) and infrared absorption spectrum for photograph JC-17 from 1100 to 1600 cm^{-1}.

Samples JC-14 and JC-15 present similar spectra, as shown in figure 12. The strong signals at 1648, 1275, and 840 cm^{-1}, characteristic of cellulose nitrate indicate that these two samples contain collodion, but not as an emulsion binder, as discussed in the following: (1) In this case we notice the absence of the baryta layer. (2) Also noteworthy is the presence of other strong absorption bands. In the first place, we can notice the presence of a compound of proteinic nature by the strong signals at 1648, 1491, 1427, and 1377 cm^{-1} related to the different amide groups, although they do not present the same spectral pattern as the other samples. (3) If we stop at the intensities of the amide III-related peaks (1427 and 1377 cm^{-1}, being the latter stronger) we can identify also the presence of albumin binder.

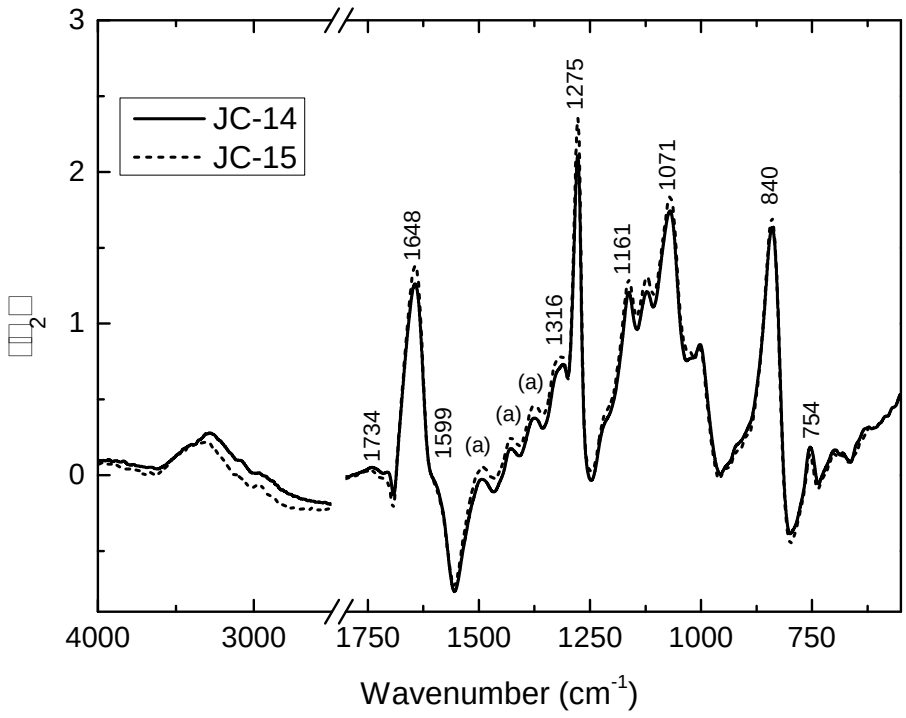

Figure 12. IRSE spectra of the photographs JC-14 and JC-15 contain collodion binder; peak label as (a) corresponds to albumen.

On the other hand, if we consider the asymmetric stretching absorption band at 1734 cm^{-1}, and the absorption bands at 1599, 1316, 1161, 1071, 840, and 754 cm^{-1} we are led to consider the possibility of a coating layer made of a mixture of collodion and camphor. Although collodion had been used mainly as the binder element in the photographic emulsion, there are previous studies that indicate its application also as part of a coating layer, especially in albumin processes (D. C. Stulik and Kaplan 2013). Consequently, samples JC-14 and JC-15 can be classified as albumen print with collodion coating. It is important to note that despite proceeding from the same photographic capture, these samples do not show the same aesthetic particularities (brightness, color, format, etc.) and the arrangement in the secondary support is different in each case. Although the aesthetic differences, the vibrational spectra are practically the same, with only slight differences in the intensities of some signals, as seen in figure 12, which clearly suggest the employment of the same materials, and very likely in the same strata. The fact that the JC-15 signal falls below the detection threshold

below 610 cm^{-1}, and the different line broadening for wavenumbers around 3000 cm^{-1}, might hint to slightly different methods of preparation, possibly the collodion coating layer thickness.

The composition and thickness of a particular layer of the photographic structure can be resolved with aid of a model mediated ellipsometry analysis, this provides an advantage over infrared spectrometry: a further source of information can be provided by the capability the instrument of measuring spectra at different angles of incidence, as, in this way the probing light travels different paths within the sample. This is cast in the form of different behaviors of peaks in the form of apparent shifts and intensity changes. In figure 13 we contrast the results of two different samples, JC-15 and JC-18. Although both contain collodion, it is used, however, for different purposes: in JC-18, in which a baryta layer was detected, the collodion forms part of the emulsion layer. On the other hand, in JC-15 it is used as a coating of the albumen layer. Figure 13 shows the real and imaginary parts of the infrared ellipsometry spectra for samples JC-15 and JC-18 recorded at different angles of incidence. For the following discussion, consider that if some differences are observed for spectra recorded at different angles of incidence, then the presence of stratified media can be safely inferred (the opposite is not necessarily true). For JC-15 the spectra are nearly independent of angle of incidence, however, some dispersion can be observed outside the collodion absorption bands (i.e., outside the vicinity of the vertical lines in Figure 13). This dispersion slightly covers the region around the amide peaks, which indicates that the albumen layer is located beneath a thin collodion capping layer. For JC-18 we observed evident changes in intensities and even apparent shifts of the bands assigned to baryta as a function of the incident angles for both, the real and imaginary parts of the infrared ellipsometry spectrum. This large dispersion of spectra indicates that (*i*) the baryta layer is flat enough as to produce wave interference, (*ii*) the baryta layer is buried under the collodion and (*iii*) it is located a few micrometers below surface. The last observation is consistent with the localization of baryta at a depth grater that 4 micrometers determined by our confocal Raman studies.

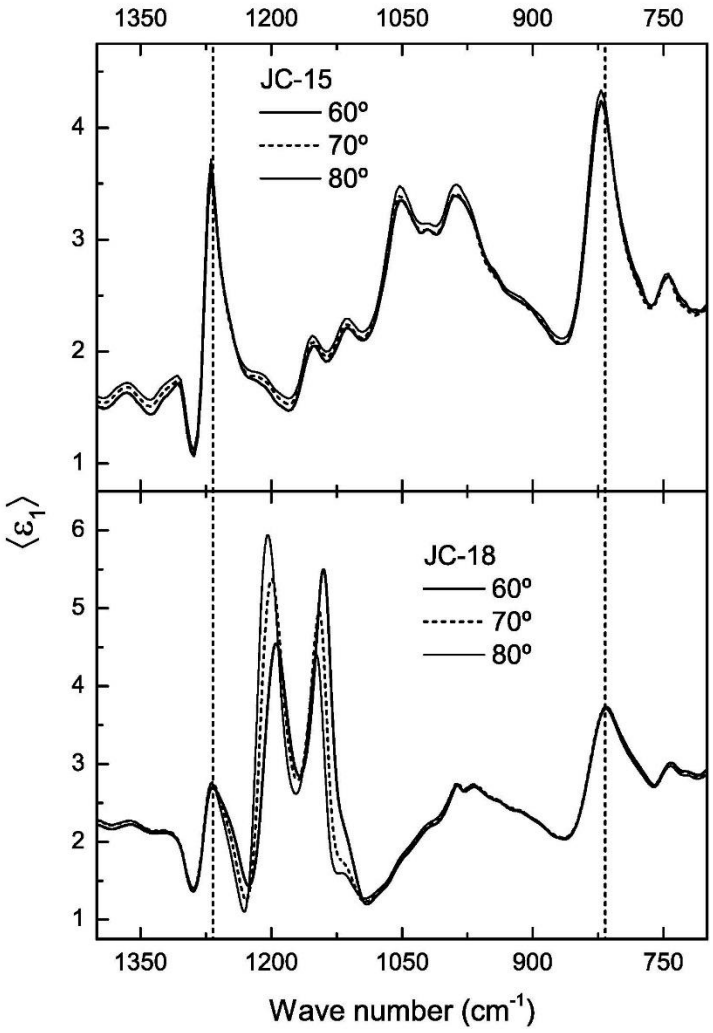
1350
1200
1050
900
750
JC-15
60°
70°
80°
JC-18
60°
70°
80°
⟨ε1⟩
Wave number (cm-1)

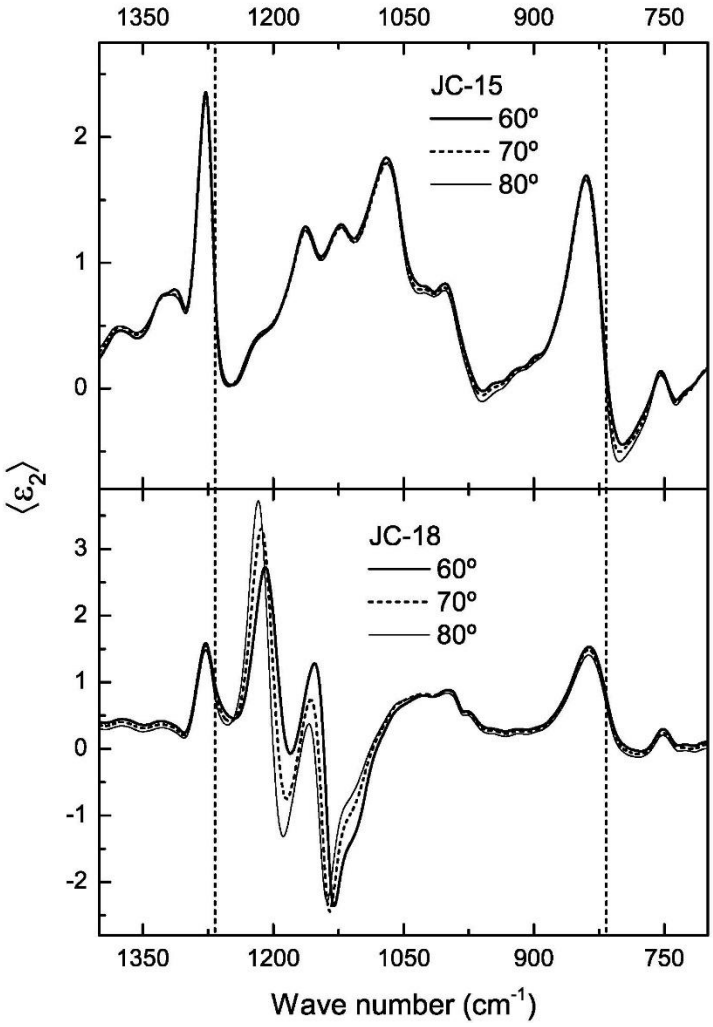

Figure 13. Real, $\langle \varepsilon_1 \rangle$, and imaginary, $\langle \varepsilon_2 \rangle$, parts of the infrared ellipsometry spectrum of photographs JC-15 and JC-18 recorded for the indicated angles of incidence, in the spectral region from 700 to 1400 cm^{-1}. The vertical lines show the positions of collodion peaks.

The baryta layer below the collodion binder layer, can be observed by measurement of micro-Raman spectroscopy in representative regions of the photograph. Figure 14 shows Raman spectra for the sample JC-16 identified as collodion print. In the selected points we show the presence of baryta. In the darker region, located at the bottom-right of the microscope image in figure 14, the peak corresponding to baryta is obscured by fluorescence characteristic of

organic compounds. In this spectrum the intensity is about ten times as high as the Raman intensity of the other points. Collodion was not detected by micro-Raman spectroscopy with our available excitation pump of 633 nm, this precludes obtaining stratigraphic information by performing a vertical cross-section. Thus, the method to estimate the baryta depth consisted on spatially scanning into the sample in the direction normal to the surface taking as a base reference the vertical position where the optical microscope was focused.

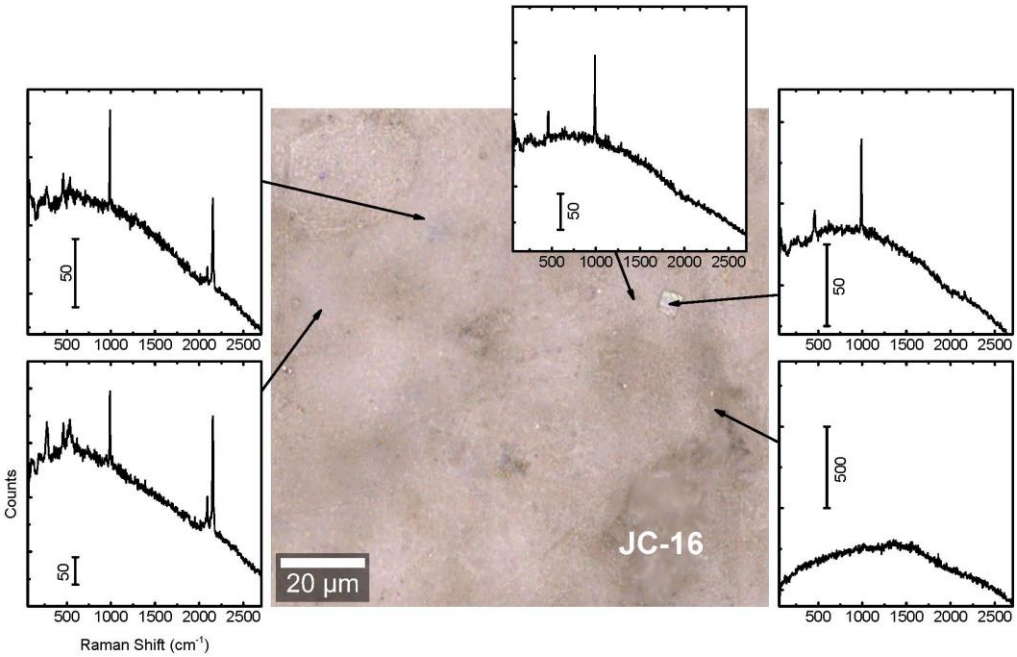

Figure 14. Characteristic Raman spectra of baryta for representative regions of photograph JC-16.

From these results, we can propose a flowchart to discriminate and identify the kind of print, and the presence of coating and plasticizer used in ancient photographic print process. The first step leads to the identification of the binder by using the following criteria: (1) compare the relative intensities of bands related with amide III, (2) locate the spectral position of the band associated to amide I, and (3) examine the presence or absence of baryta layer. Hence, we can determine the kind of binder print as gelatin, albumen or collodion. Furthermore, in the case of gelatin binder, we can also differentiate print processes depending on whether the baryta layer is detected or not. In one of the analyzed cases it was possible to identify a carbon

print process. The second step consists on determining the presence of a coating layer. In the case of gelatin, the presence or absence of a coating can be detected by infrared contribution at about 1730 cm^{-1}, the kind of the employed natural organic component can be determined by analyzing its characteristic functional groups vibrations in the region for OH stretches, methyl and methylene stretches, carbonyl bands and the fingerprint region below 1800 cm^{-1} due to C-H, C-O and C-C wags and bends. The shellac presence was determined with the peak at 1221 cm^{-1}. Similarly, we can determine presence of coating for the case of collodion print and albumen print. The flowchart is schematized in figure 15. We mention in the flowchart a special case labeled “other print” as possible photograph process, where we detected albumen and strikingly a baryta layer. This seemingly contradictory case, corresponds in fact to a collodion print with albumen coating. Step 2 in figure 15 refers to the flowchart proposed by Daher et al. (2010). This step is useful for the determination of the natural organic components, such resins, oils, waxes, glues or gums, of a coating layer, by means of infrared and Raman spectroscopies.

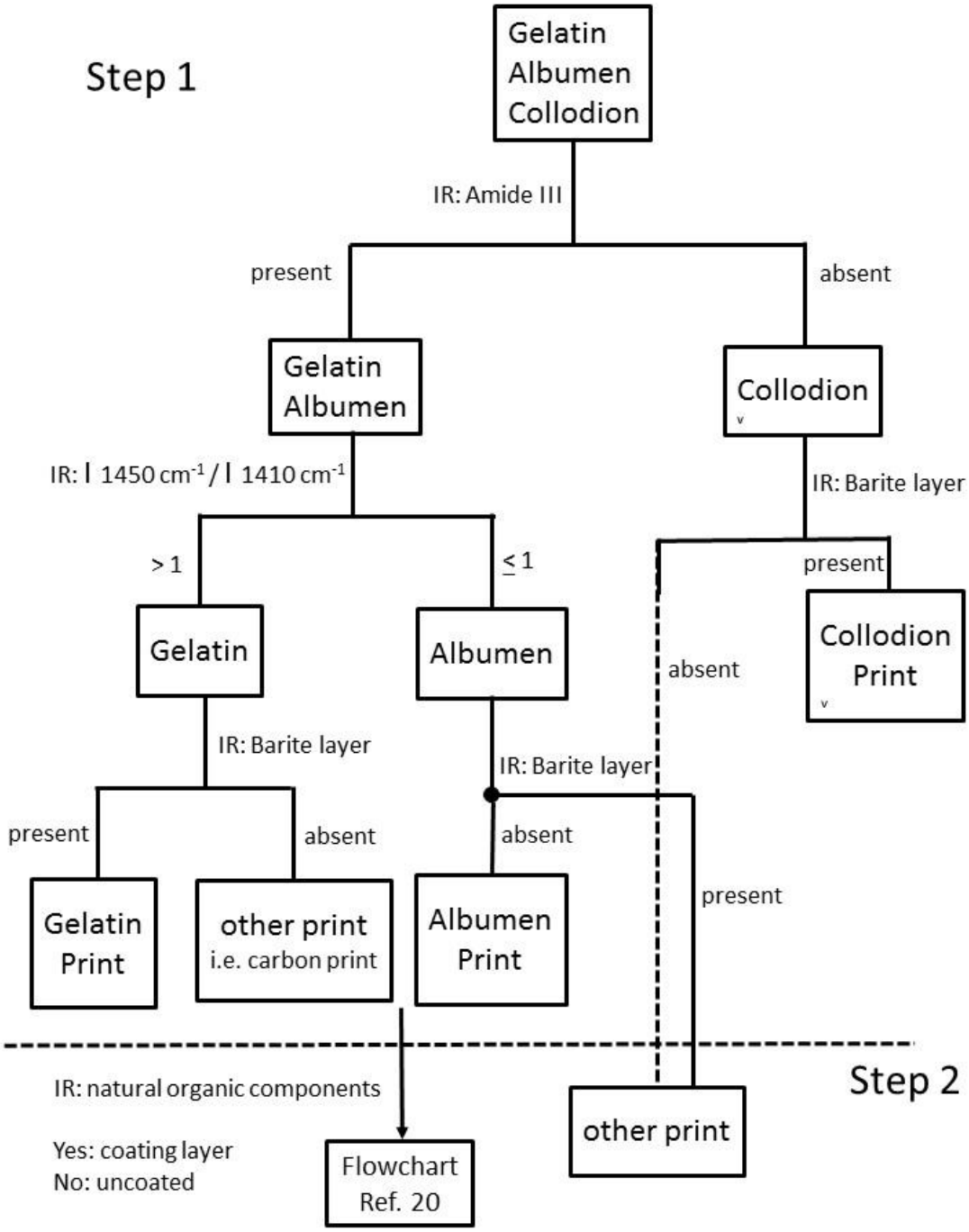

Figure 15. Flowchart proposed to discriminate and identify the kind of print, the presence of coating and plasticizer used in ancient photographic print process.

Its use allowed us to have an almost complete description of the composition in ancient photography by identifying coatings and determining the presence of the baryta layer between the layer that contains the binder and the paper support, complementing the results of previous works where infrared spectroscopy is used.

From the present results we can conclude that infrared spectroscopic ellipsometry have some advantages over infrared spectroscopy such as its capability of, besides resolving the infrared-active absorption bands, distinguishing individual layers in a stratified system such as the photographic prints, which is achieved by measuring changes in the polarization state in contrast to intensities attenuations, thus, the acquired data carry information only from the sample without being affected by the surrounding environment, such as ambient air. The apparent complexity of ellipsometry spectra manifested by the occasional interchange of real and imaginary parts of the dielectric functions of individual layers depending on both, angle of incidence and spectral region, is, in fact, a highlight of the degree of sensitivity of this technique: this is the key to obtain information on the layered structure of photograph prints. Furthermore, the behavior of baryta peaks for different angles of incidence permits (1) its unambiguous distinction from e.g., the cellulose of the support, whose absorption bands may coincide with and even overcome those of baryta in FTIR-ATR as observed in other reports (Ricci, Bloxham, and Kazarian 2007; Vila and Centeno 2013; Cattaneo et al. 2008) and (2), subsequently, an estimation of its depth in the photographic structure.

A disadvantage of IRSE as compared to FTIR, is its lack of spatial resolution, since the diameter of the light spot of our instrument is of the order of 1 cm, which prevented us from performing, for instance, an analysis of dark and light regions of the photograph.

4. Conclusions

By using infrared spectroscopic ellipsometry (IRSE) we were able to characterize photographic prints form the turn of the 20th century. With this noninvasive technique we can identify the presence of the kind of binder, the coating layer, and the plasticizer, besides of unambiguously detecting the presence of the baryta layer, and resolving the contribution of

absorption bands in the spectral region below 1400 cm^{-1} in which it is common to observe loss of resolution in techniques using diffuse reflectance. From the results presented in this work, we propose a flowchart that permit us to classify the kind of print as gelatin, collodion, albumen or carbon print, and to determine whether a coating layer was deposited or not. In particular for the set of photographs belonging to the Carrillo archives, we classified the samples JC-03, JC-05, JC-20 and JC-29 as gelatin print without coating, the sample JC-12 as gelatin print with shellac coating, the sample JC-04 as carbon print, the sample JC-13 as albumen print with beeswax coating, the samples JC-14 and JC-15 as albumen print with collodion coating, the samples JC-16, JC-18 and JC-19 as collodion print with camphor and the sample JC-17 as albumen print with unknown protective coating, possible Arabic gum (i. e. gum bichromate print).

Referencia tabla (Nieto-Villena et al. 2018)

References

Brambilla, L., C. Riedo, C. Baraldi, A. Nevin, M. C. Gamberini, C. D'Andrea, O. Chiantore, S. Goidanich, and L. Toniolo. 2011. "Characterization of Fresh and Aged Natural Ingredients Used in Historical Ointments by Molecular Spectroscopic Techniques: IR, Raman and Fluorescence." *Analytical and Bioanalytical Chemistry* 401 (6): 1827–1837. doi:10.1007/s00216-011-5168-z.

Casoli, Antonella, and Silvia Fornaciari. 2014. "An Analytical Study on an Early Twentieth-Century Italian Photographs Collection by Means of Microscopic and Spectroscopic Techniques." *Microchemical Journal* 116. Elsevier B.V.: 24–30.

Cattaneo, Barbara, David Chelazzi, Rodorico Giorgi, Tiziana Serena, Curzio Merlo, and Piero Baglioni. 2008. "Physico-Chemical Characterization and Conservation Issues of Photographs Dated between 1890 and 1910." *Journal of Cultural Heritage* 9 (3): 277–284.

Coe, Brian, and Mark Haworth-Booth. 1983. *A Guide to Early Photographic Processes*. The Victoria and Albert Museum in association with Hurtwood Press.

Daher, Céline, Céline Paris, Anne-Solenn Le Hô, Ludovic Bellot-Gurlet, and Jean-Philippe

Échard. 2010. “A Joint Use of Raman and Infrared Spectroscopies for the Identification of Natural Organic Media Used in Ancient Varnishes.” *Journal of Raman Spectroscopy* 41 (November 2010): 1494–1499. doi:10.1002/jrs.2693.

Derrick, Michele. 1989. “Fourier Transform Infrared Spectral Analysis of Natural Resins Used in Furniture Finishes.” *Journal of the American Institute for Conservation* 28 (1): 43. doi:10.2307/3179466.

Derrick, Michele R., Dusan Stulik, and James M. Landry. 2015. *Infrared Spectroscopy in Conservation Science*. *The Effects of Brief Mindfulness Intervention on Acute Pain Experience: An Examination of Individual Difference*. Vol. 1. doi:10.1017/CBO9781107415324.004.

Edwards, H.G.M., D.W. Farwell, and L. Daffner. 1996. “Fourier-Transform Raman Spectroscopic Study of Natural Waxes and Resins. I.” *Spectrochimica Acta Part A: Molecular and Biomolecular Spectroscopy* 52 (12): 1639–1648. doi:10.1016/0584-8539(96)01730-8.

Fujiwara, Hiroyuki. 2007. *Spectroscopic Ellipsometry Principles and Applications*. Edited by LTD John Wiley & Sons. http://cds.cern.ch/record/1086851/files/0470016086_TOC.pdf.

Gernsheim, Helmut. 1965. *A Concise History of Photography*. General Pu. Toronto: Dover Publications.

Golovlev, VV, MJ Gresalfi, JC Miller, and D Anglos. 2003. “Laser Characterization and Cleaning of 19th Century Daguerreotypes II.” *Journal of Cultural*. http://www.sciencedirect.com/science/article/pii/S1296207402011895.

Hendriks, Klaus B., and Lincoln Ross. 1988. “Chemical Treatments of Discoloured Photographic Prints : Image Manipulation or Legitimate Restoration?” *Journal of Photographic Science* 36 (3): 132. http://www.bcin.ca/Interface/openbcin.cgi?submit=submit&Chinkey=191599.

Hogan, DL, VV Golovlev, and MJ Gresalfi. 1999. “Laser Ablation Mass Spectroscopy of Nineteenth Century Daguerreotypes.” *Applied*. https://www.osapublishing.org/abstract.cfm?uri=as-53-10-1161.

Mallégol, Jacky, Jean-Luc Gardette, and Jacques Lemaire. 2000. “Long-Term Behavior of Oil-Based Varnishes and Paints. Photo- and Thermooxidation of Cured Linseed Oil.”

Journal of the American Oil Chemists' Society 77 (3). Springer-Verlag: 257–263. doi:10.1007/s11746-000-0042-4.

McCabe, Constance. 2005. *Coatings on Photographs: Materials, Techniques, and Conservation*. American Institute for Conservation of Historic & Artistic W.

Mills, John S., and Raymond White. 1977. "Natural Resins of Art and Archaeolog. Their Sources, Chemestry, and Identification." *Studies in Conservation* 22 (1). Routledge: 12–31. doi:10.1179/sic.1977.003.

Neville, Harvey A. 1942. "Protective and Decorative Coatings, Paints, Varnishes, Lacquers, and Inks. Volume I: Raw Materials for Varnishes and Vehicles (Mattiello, Joseph J." ACS Publications.

Nieto-Villena, A., J.R. Martínez, J. A. de la Cruz-Mendoza, J.C. Valcárcel-Andrés, G. Ortega-Zarzosa, Á. Solbes-García, and E. Vázquez-Martínez. 2018. "Atomic Force Microscopy as a Tool for Binder Identification in Ancient Photographic Processes." *Surface and Interface Analysis*, no. January: 1–10. doi:10.1002/sia.6408.

Ostroff, Eugene. 1966. "Restoration of Photographs by Neutron Activation." *Science* 154 (3745). http://science.sciencemag.org/content/154/3745/119.

Othmer, Kirk. 1990. "Encyclopedia of Chemical Technology, Vol. 17 (1982)." *G. LAZAROV: Structura I Reakcii Uglej. Sofia*, 79.

Perron, Johanne. 1989. "The Use of FTIR in the Study of Photographic Materials." *Topics in Photographic Preservation* 3: 112–122.

Ramaswamy, V, R.M. Vimalathithan, and V. Ponnusamy. 2010. "Synthesis and Characterization of BaSO4 Nano Particles Using Micro Emulsion Technique." *Advances in Applied Science Research. Pelagia Research Library* 1 (3): 197–204. http://www.pelagiaresearchlibrary.com/advances-in-applied-science/vol1-iss3/AASR-2010-1-3-197-204.pdf.

Reilly, James M. 1986. *Care and Identification of 19th Century Photographic Prints*. Rochester, New York: Eastman Kodak Company.

Ricci, Camilla, Simon Bloxham, and Sergei G. Kazarian. 2007. "ATR-FTIR Imaging of Albumen Photographic Prints." *Journal of Cultural Heritage* 8 (4): 387–395.

Sammlung, Museum Folkwang Essen. Fotografische, Robert Knodt, and Klaus Pollmeier. 1999. *Verfahren Der Fotografie: Bilder Der Fotografischen Sammlung Im Museum*

Folkwang Essen.

Sifontes, Ángela B., Edgar Cañizales, Jhoan Toro-Mendoza, Edward Ávila, Petra Hernández, Blas A. Delgado, G. Brenda Gutiérrez, Yraida Díaz, and Eliandreina Cruz-Barrios. 2015. "Obtaining Highly Crystalline Barium Sulphate Nanoparticles via Chemical Precipitation and Quenching in Absence of Polymer Stabilizers." *Journal of Nanomaterials* 2015 (February). doi:10.1155/2015/510376.

Stulik, Dusan C, and Art Kaplan. 2013. *The Atlas of Analytical Signatures of Photographic Processes. Albumen. The Getty Conservation Institute*.

Stulik, Dusan, Herant Khanjian, Alberto de Tagle, and Alexandra M Botelho. 2002. "Investigation of Jean-Louis-Marie-Eugene Durieu's Toning and Varnishing Experiments: A Non-Destructive Approach." In *ICOM Committee for Conservation 13th Triennial Meeting*, 658–663. Río de Janeiro.

"The Infrared and Raman Users Group (IRUG)." 2009.

Vila, Anna, and Silvia A. Centeno. 2013. "FTIR, Raman and XRF Identification of the Image Materials in Turn of the 20th Century Pigment-Based Photographs." *Microchemical Journal* 106. Elsevier B.V.: 255–262. doi:10.1016/j.microc.2012.07.016.

Figure captions:

Figure 1. Set of 13 photographs from the Centro Julián Carrillo archives (Mexico) selected for this study.

Figure 2. IRSE spectra of the photograph JC-03 in the regions 1350 cm^{-1} to 1750 cm^{-1} a), 550 cm^{-1} to 1250 cm^{-1} b), and 2825 cm^{-1} to 3150 cm^{-1} c).

Figure 3. A) IRSE and B) FTIR spectrum of photograph JC-04. Peaks corresponding to bone black pigment are indicated with (b) labels.

Figure 4. Real, $\langle \varepsilon_1 \rangle$, and imaginary, $\langle \varepsilon_2 \rangle$, parts of the infrared ellipsometry spectrum of photographs JC-29 and JC-04 in the region between 600 cm^{-1} to 1200 cm^{-1}.

Figure 5. IRSE spectra for the photograph JC-12 in the region 1150 cm^{-1} to 1800 cm^{-1}.

Figure 6. Raman dispersion for the photographs JC-12.

Figure 7. IRSE spectra of the photograph JC-13 in the spectral region from 1350 to 1750 cm^{-1}.

Figure 8. Comparison of IRSE spectra for the photographs JC-13 and JC-29 in the spectral region from 550 to 1700 cm^{-1}.

Figure 9. IRSE spectra of the photograph JC-13 in the spectral region from 2825 to 3100 cm^{-1}.

Figure 10. IRSE spectra of the photograph JC-16 in the spectra region from 550 to 1800 cm^{-1}.

Figure 11. A) Real $\langle \varepsilon_1 \rangle$, and imaginary $\langle \varepsilon_2 \rangle$ parts of the infrared ellipsometry spectrum of photograph JC-17 in the spectral region from 600 to 1700 cm^{-1}, and B) and infrared absorption spectrum for photograph JC-17 from 1100 to 1600 cm^{-1}.

Figure 12. IRSE spectra of the photographs JC-14 and JC-15 contain collodion binder; peak label as (a) corresponds to albumen.

Figure 13. Real, $\langle \varepsilon_1 \rangle$, and imaginary, $\langle \varepsilon_2 \rangle$, parts of the infrared ellipsometry spectrum of photographs JC-15 and JC-18 recorded for the indicated angles of incidence, in the spectral region from 700 to 1400 cm^{-1}. The vertical lines show the positions of collodion peaks.

Figure 14. Characteristic Raman spectra of baryta for representative regions of photograph JC-16.

Figure 15. Flowchart proposed to discriminate and identify the kind of print, the presence of coating and plasticizer used in ancient photographic print process.